Journal of Structural Geology 74 (2015) 64–80

Contents lists available at ScienceDirect

Journal of Structural Geology

journal homepage: www.elsevier.com/locate/jsg

Influence of structural position on fracture networks in the Torridon Group, Achnashellach fold and thrust belt, NW Scotland

Hannah Watkins*, Robert W.H. Butler, Clare E. Bond, Dave Healy

Geology & Petroleum Geology, School of Geosciences, University of Aberdeen, Kings College, Aberdeen, AB24 3UE, UK

ARTICLE INFO

Article history:
Received 17 December 2014
Received in revised form
19 February 2015
Accepted 1 March 2015
Available online 10 March 2015

Keywords:
Fracture
Strain
Structural position
Tight sand
Fold and thrust belt

ABSTRACT

In fold-and-thrust belts rocks undergo deformation as fold geometries evolve. Deformation may be accommodated by brittle fracturing, which can vary depending on structural position. We use 2D forward modelling and 3D restorations to determine strain distributions throughout folds of the Achnashellach Culmination, Moine Thrust Belt, NW Scotland. Fracture data is taken from the Torridon Group; a thick, coarse grained fluviatile sandstone deposited during the Proterozoic. Modelling infers a correlation between strain and simple curvature; we use simple curvature to infer how structural position and strain control fracture attribute variations in a fold and thrust belt.

In high curvature regions, such as forelimbs, fracture intensities are high and fractures are short and oriented parallel to fold hinges. In low curvature regions fractures have variable intensities and are longer. Fracture orientations in these regions are scattered and vary over short distances. These variations do not relate to strain; data suggests lithology may influence fracturing. The strain history of fold structures also influences fracturing; structures with longer deformation histories exhibit consistent fracture attributes due to moderate-high strain during folding, despite present day low curvature. This is in contrast to younger folds with similar curvatures but shorter deformation histories. We suggest in high strain regions fracturing is influenced by structural controls, whereas in low strain regions lithology becomes more important in influencing fracturing.

© 2015 The Authors. Published by Elsevier Ltd. This is an open access article under the CC BY license (http://creativecommons.org/licenses/by/4.0/).

1. Introduction

Fractures in fold and thrust belts are often thought to form synchronously with folding and therefore fracture pattern variations may be expected to relate to structural position on the fold. Understanding the mode of fold formation and strain history is critical for prediction of fracture attribute variations, which can be used in a range of applications, including fractured reservoir exploration, carbon capture and storage, aquifer characterisation and civil and mining engineering. Many studies have been conducted to investigate how fracture attributes vary in carbonate thrust belts for hydrocarbon exploration, such as in the Zagros fold-and-thrust belt of Iran (McQuillan, 1973, 1974; Wennberg et al., 2006; Wennberg et al., 2007; Awdal et al., 2013), the Italian Apennines (Storti and Salvini, 2001), the Rocky Mountains of the USA and Canada (Ghosh and Mitra, 2009; Barbier et al., 2012) and the Northeastern Brooks Range, Alaska (Hanks et al., 1997). Studies on fracturing in sandstone thrust belts are much less well documented; examples include Florez-Niño et al. (2005) and Iñigo et al. (2012) who use fractured outcrops as analogues to low porosity, low permeability (tight) sandstone hydrocarbon reservoirs in the Sub-Andean thrust belt. Other examples include Hennings et al. (2000), Bergbauer and Pollard (2004) and Bellahsen et al. (2006), who investigate fracture distributions across sandstone anticlines in Wyoming, USA, and Guiton et al. (2003) determine fold-fracture relationships in folded Devonian sandstones, Morocco. This paper contributes to the limited studies on fracturing in sandstone thrust belts, using the Torridon Group of the Moine Thrust Belt, NW Scotland as an analogue for a tight fractured sandstone reservoir in a fold and thrust belt.

Fracture variations have been attributed to both structural and lithological controls (e.g. Nelson, 1985). It is widely acknowledged that fracture set orientation within a deformed region relates to the orientation of principle stresses during the formation of those

* Corresponding author. Tel.: +44 1224 273519.
E-mail addresses: h.watkins@abdn.ac.uk (H. Watkins), rob.butler@abdn.ac.uk (R.W.H. Butler), clare.bond@abdn.ac.uk (C.E. Bond), d.healy@abdn.ac.uk (D. Healy).

http://dx.doi.org/10.1016/j.jsg.2015.03.001
0191-8141/© 2015 The Authors. Published by Elsevier Ltd. This is an open access article under the CC BY license (http://creativecommons.org/licenses/by/4.0/).

fractures. In a thrust related anticline we may expect to see up to four fracture sets (Price, 1966); the first being a joint set striking parallel to the fold hinge and dipping normal to bedding (J1, Fig. 1). This fracture set may be associated with outer-arc stretching during folding; regions of localised tensional stresses develop in the same orientation as regional compression, leading to fracture opening. A second joint set strikes perpendicular to the fold hinge and dips normal to bedding (J2, Fig. 1). This fracture set may be associated with localised extension due to elevated curvature on a plunging anticline.

The remaining fractures associated with a thrust related anticline are two sets of conjugate shear fractures (S1 & S2, Fig. 1) with an acute bisector parallel to the thrust transport direction. These fractures may form due to regional compression or localised inner-arc compression associated with tangential longitudinal strain folding (Ramsay, 1967). Often incomplete assemblages of these fractures are seen at outcrop where not all of the four fracture sets have developed. Cooper (1992) describes well developed J1 and J2 fractures parallel and perpendicular to the fold hinge and normal to bedding in the Upper Triassic Pardonet dolomites in the regions of the Sukunka and Bullmoose gas fields in NE British Columbia. Bedding-normal joints striking parallel to the fold hinge (J1) are documented alongside conjugate shear fractures with an acute bisector parallel to the transport direction (S1 & S2) (Muecke and Charlesworth, 1966) in folded Cardium Sandstones of the Canadian Rocky Mountain foothills. Complete fracture set assemblages have been documented from field examples such as in the Umbria-Marche Apennines (Di Naccio et al., 2005) and on the Khaviz anticline, SW Iran (Wennberg et al., 2007).

If fractures are stratabound (i.e. fracture height does not exceed the thickness of the mechanical layer within which the fracture has developed (Odling et al., 1999)), the height of a fracture is limited by the mechanical layer thickness (e.g. Wennberg et al., 2006), which limits fracture length (the exact relationship between mechanical layer thickness and fracture length depends on the aspect ratio of fracture length to height). Fracture length may also be structurally controlled; if strain increases during folding fractures may propagate in order to accommodate this strain. This would, in theory, lead to longer fractures in higher strained zones (Fig. 1); this relationship is shown by Ghosh and Mitra (2009) who calculate higher average fracture lengths in hinges than limbs. Fracture apertures may be controlled by strain; fracture widening accommodates increasing strain during folding, therefore we may expect to find wide apertures in high strain zones (Jamison, 1997) (Fig. 1). This relationship is seen in the Sub-Andean fold and thrust belt (Iñigo et al., 2012) where fracture apertures widen from the low strain backlimbs to the higher strain hinge and forelimbs. Fracture aperture is also though to correlate to fracture lengths; longer fractures tend to have wider apertures. This relationship is shown by Vermilye and Scholz (1995) who use many field locations across North America, and Ellis et al. (2012) who use data from the Torridon Group of NW Scotland.

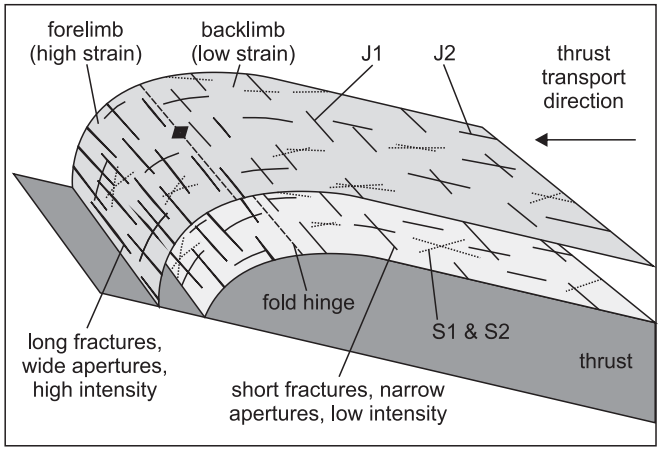

Fig. 1. Expected fracture characteristics on a thrust-related anticline. Steeper-dipping forelimbs are thought to have undergone higher strain meaning that fractures are better developed; fractures are longer and have high intensities in these regions. Four fracture sets are expected on thrust related anticlines; orientations relate to fold geometries and regional thrust transport direction (Price, 1966).

Controls on fracture intensity (fracture length per unit area in 2D) have been widely investigated through field-based studies. Many authors attribute variations in fracture intensity to rock strength and brittleness, which are controlled by rock composition, texture, grain size and porosity (e.g. Hugman and Friedman, 1979). Rocks with low competency such as clay-rich chalk, limestone or dolomite (Corbett et al., 1987; Ferrill and Morris, 2008) are often associated with low fracture intensities. Higher competency rocks such as dolomite-rich carbonates are associated with much higher fracture intensities (Barbier et al., 2012; Ferrill and Morris, 2008; Hanks et al., 1997; Hugman and Friedman, 1979; Ortega et al., 2010) as dolomite is a brittle mineral. Porosity is also seen to affect fracture intensity. In many cases higher fracture intensities are found in low porosity, high density rocks (e.g. Ameen, 2014), whereas in other examples higher porosities are associated with higher fracture intensities in carbonates (e.g. Barbier et al., 2012). Correlations are also seen between fracture intensity and carbonate grain size (Hanks et al., 1997; Hugman and Friedman, 1979), although this may be because coarser grained sedimentary rocks tend to be deposited with lower mud and clay content than finer grained rocks. As well as lithology, bed thickness is thought to influence fracture intensity; Mitra (1988) shows that fracture intensity is generally higher in thin beds.

Evidence for fracture intensity being structurally controlled is also seen; Bergbauer and Pollard (2004) report 5–10 times higher fracture intensities in folded sandstones & shales than in unfolded regions, although intensity values are constant on the fold itself. McQuillan (1973) also suggests fracture density is constant within fold structures of the Asmari Formation, SW Iran, providing bed thickness and lithology are constant. Many studies show an increase in fracture intensity in high curvature and high strain regions of individual fold structures in a range of lithologies (Hobbs, 1967; Jamison, 1997; Ortega et al., 2010), for example fracture intensity is often seen to be higher in fold forelimbs and crests than backlimbs (Barbier et al., 2012; Awdal et al., 2013).

We investigate variations in fracture set orientation, length, aperture, spatial distribution and intensity in a deformed tight (low matrix porosity and permeability) sandstone. We aim to determine whether fracture patterns are systematically structurally controlled within a fold and thrust belt, and therefore vary depending on their structural position.

2. Achnashellach Culmination

The Achnashellach Culmination is used as a field location for fracture data collection. The culmination is a fold-and-thrust belt in the southern Moine Thrust zone (Fig. 2b), which formed during the Caledonian Orogeny (c. 439-410 Ma, Mendum et al., 2009). Up to eight large-scale thrust-related anticlines of Torridon Group and Cambro-Ordovician sedimentary rocks (Basal Quartzite, Pipe Rock, Fucoid Beds, Salterella Grit and Durness Group) are exposed within a narrow, 3.5 km wide zone (Fig. 2a). The Achnashellach

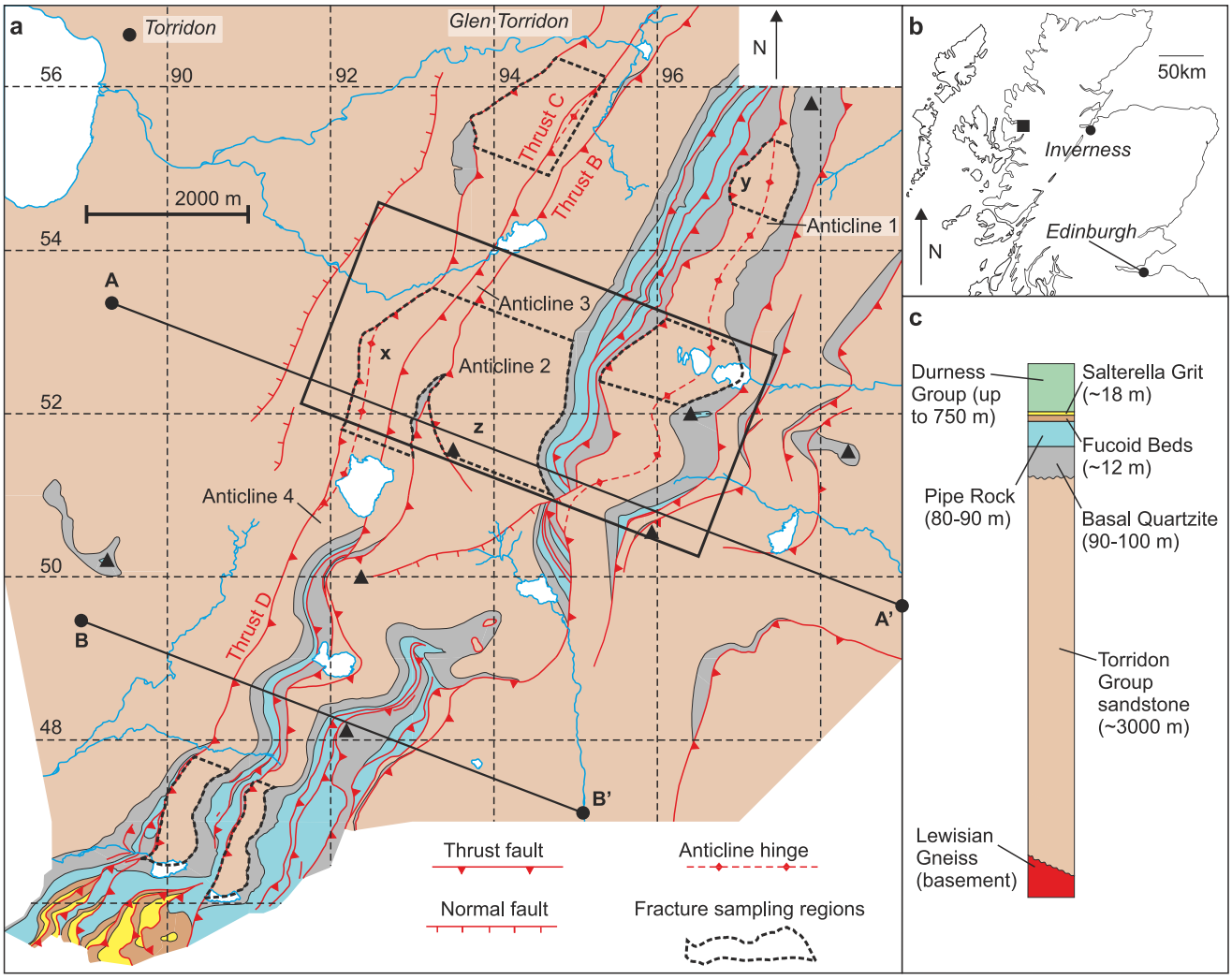

Fig. 2. **a**. Geological map of the Achnashellach Culmination showing fracture sampling regions presented in this region, section traces (A–A′, B–B′) and 3D model extent (black rectangle). **b**. Map showing the location of the Achnashellach Culmination (black square) in NW Scotland. **c**. Key to Geological map showing the stratigraphy of the Southern Moine Thrust Belt.

Culmination contains the highest relief of the entire thrust belt (up to 1000 m vertical sections), allowing detailed mapping of thrust geometries and determination of a thrusting history (Fig. 3a). Deformation in the Achnashellach Culmination is dominated by brittle fracturing. *Skolithos* trace fossils in the Pipe Rock remain unsheared, indicating very little internal deformation. A lack of crystal-plastic deformation suggests folding and thrusting occurred under cool ambient temperatures (Butler et al., 2007).

Folding and thrusting of the Achnashellach Culmination is thought to have formed within the footwall of the Kishorn/Kinlochewe Thrusts, which are structurally below the Moine Thrust (Butler et al., 2007). Large scale folds formed from a detachment horizon within the Torridon Group (Butler et al., 2007; Watkins et al., 2014) in a WNW directed foreland propagating thrust sequence (see Watkins et al., 2014 for a discussion of the fold and thrust evolution history and structural restorations).

A 3D model of the sampling area, colour mapped for simple curvature, is shown on Fig. 4 (see Fig. 2a for model extent). Two types of fold curvature can be measured; simple curvature and gaussian curvature. Gaussian curvature is a measure of the degree of double curvature (Lisle, 2000), and is the sum of two principle curvatures (usually parallel and perpendicular to the hinge on a fold). This means a cylindrical fold, where one principle curvature equals zero (i.e. curvature along the fold hinge), will have a Gaussian curvature of zero (Lisle, 1994). Simple curvature is a measure of rate of change of dip, measured in the direction of maximum dip (e.g. Hennings et al., 2000), meaning the simple curvature value for a cylindrical fold can be greater than zero. The model (Fig. 4) shows that the four folds sampled in this study have variable geometries; the oldest anticline sampled (Anticline 1) has straight limbs (simple curvature: 0.00–0.03) and a narrow, moderate simple curvature hinge zone (simple curvature: 0.03–0.06). Anticlines 2 and 3 have straight, low simple curvature backlimbs (simple curvature: 0.00–0.03); forelimb and hinges are not exposed. The youngest anticline (Anticline 4) has a high simple curvature forelimb in which bedding is often overturned (simple curvature: 0.06–0.14), and an un-curved backlimb (simple curvature: 0.00–0.03).

The Torridon Group sandstone is used to study fractures on the four youngest anticlines of the Achnashellach Culmination as it is well exposed within the chosen sampling areas (Fig. 3b) and provides a suitable analogue for tight sand reservoirs. The Torridon

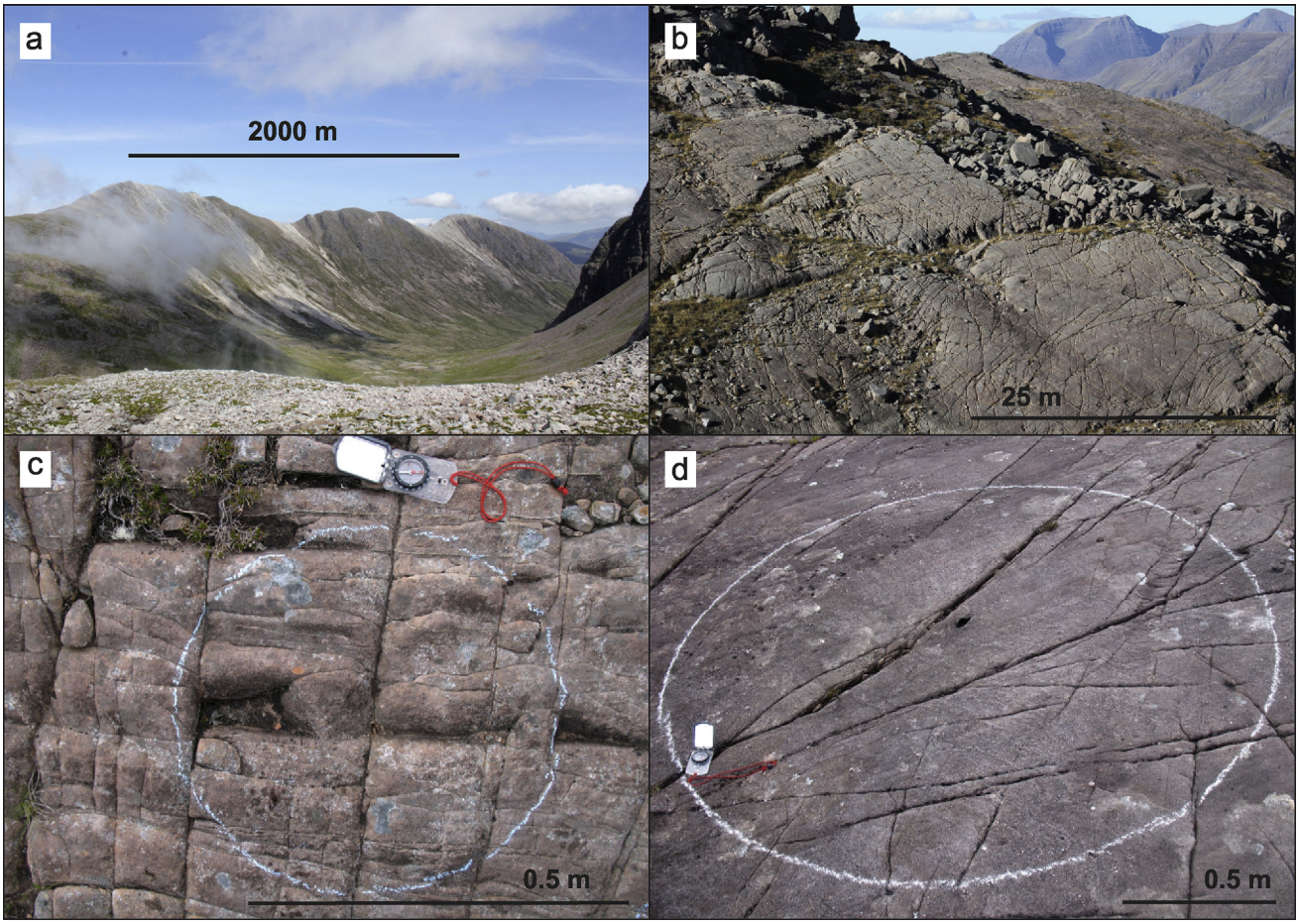

Fig. 3. **a**. High relief in the Achnashellach Culmination allows for detailed mapping of thrust and fold geometries in Torridon Group sandstone, Basal Quartzite and Pipe-Rock. **b**. Well exposed bedding planes of Torridon Group sandstone provide a suitable study area for fracture data collection. **c**. High intensity, orthogonal fracture sets on a Torridon Group bedding plane. **d**. Low intensity fractures with irregular orientations; variations in fracture attributes (e.g. compared to Fig. 3c) mean that the Achnashellach Culmination is an ideal area to investigate controls on fracturing.

Group is a low porosity, low permeability, sandstone, deposited in large braided river systems during the Proterozoic (c. 1024 Ma) (Stewart, 2002). Within the study area the Torridon Group is made up of thick beds (1–5 m) of coarse grained, cross bedded sandstones. The Torridon Group is composed of roughly 45–55% quartz, 25% plagioclase and orthoclase, 15–20% clays (illite and chlorite) and minor proportions of muscovite mica (Stewart, 2002). Individual beds of Torridon Group sandstone show only limited average grain size variations, which is ideal for fracture data collection to determine structural control as it reduces the chances of fracture variations due to bed anisotropy. Torridon Group bedding planes within the study area show significant variations in fracture orientations, lengths, apertures, spatial distribution and intensity throughout the fold structures (e.g. Fig. 3c–d), making this an ideal area to study controls on fracture formation.

3. Data collection

3.1. Methods

Fracture data is collected from over 140 sampling sites within a 7 km^2 area on the four youngest anticlines of the Achnashellach Culmination (see Fig. 2a for sampling regions). Data collection regions are selected from aerial photographs where Torridon Group bedding plane outcrops are extensive, well exposed and accessible. The sampling regions are then gridded using a 200 m grid-square system where sampling sites are at, or as close as possible to, the corners of each grid square. In order to investigate higher resolution variations in fracture attributes additional sampling sites are selected along linear transects either parallel to the regional transport direction or parallel to the fold hinge. These sampling sites are spaced 10–100 m apart, often on the same bedding plane as neighbouring sampling sites (for a full description of sampling site selection workflow, refer to Watkins et al., 2015).

At each pre-selected sampling site a circle of known radius is drawn onto the outcrop in chalk. The orientation, length, aperture and spacing (distance to nearest fracture of the same orientation) are recorded for each fracture intersecting the sampling circle, and average grain size is recorded from within the circle. The number of fracture intersections with the circle (n) is also recorded; values for n are used to estimate bulk fracture intensity at each sampling site using equation (1) (Mauldon et al., 2001).

$$I = n/(4r) \quad (1)$$

Where I = fracture intensity (m/m^2), n = number of fracture intersections with the sampling circle, and r = circle radius (m). (Mauldon et al., 2001).

This data collection method is favoured over other techniques such as linear scan line sampling (Priest and Hudson, 1981; Priest, 1993) and window sampling (Pahl, 1981; Priest, 1993) as it allows

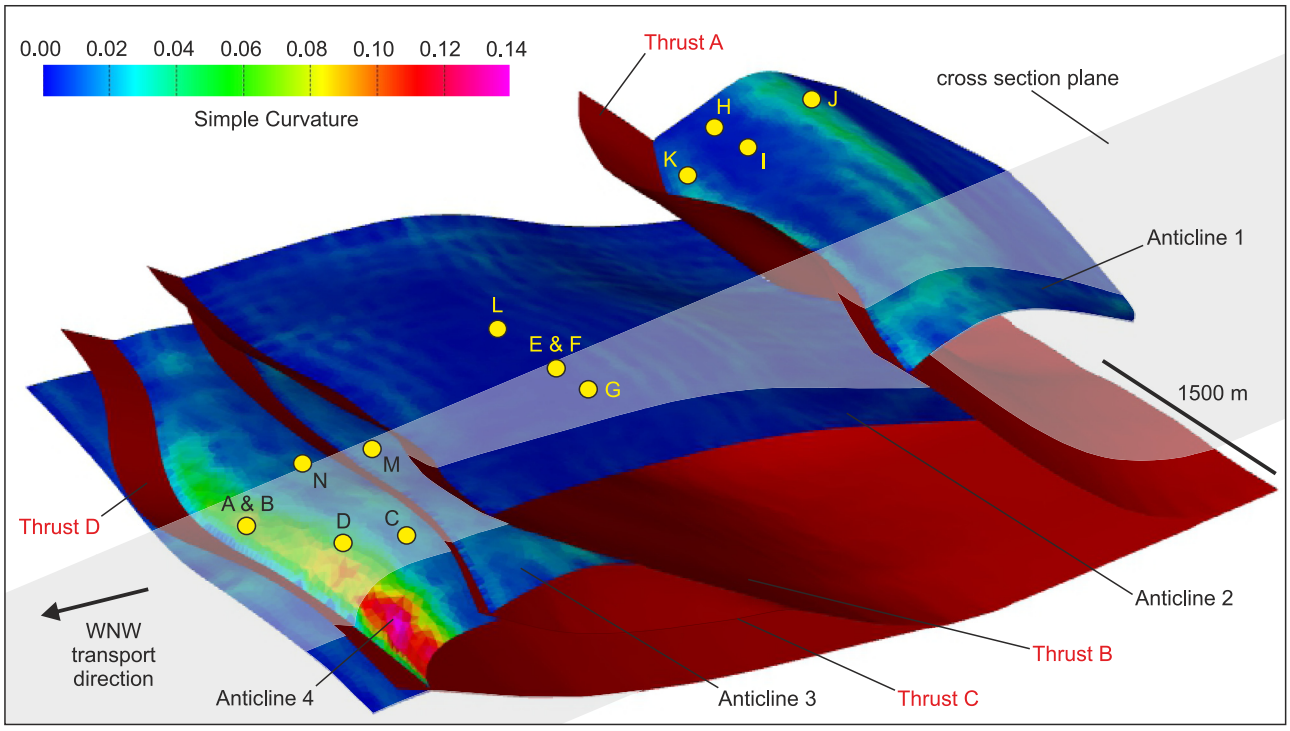

Fig. 4. 3D diagram created using Move software, showing the geometries and variations in simple curvature of the four folds discussed in this paper. Cross section plane A–A′ is shown, sampling sites are shown at their correct structural positions (yellow circles). See Fig. 2a for map location of 3D model.

for rapid data collection of a range of fracture attributes without incurring any orientation bias (see Watkins et al., 2015; for appraisal of fracture sampling techniques). Sampling circle radii varied depending on fracture intensity; minimum *n* counts of 30 were required to ensure results were representative (see Watkins et al., 2015). Circle radii range from 0.25 m in the highest fracture intensity regions to 2 m in very low intensity regions.

Bedding data collected in the field is used to construct a series of parallel cross sections representing fold geometries of the Torridon Group. From these cross sections 3D models are created (e.g. Fig. 4), from which simple curvature of the folds can be determined for each sampling site. Simple curvature values are compared with fracture attribute data to infer any relationship between fracturing and structural position. Strain, calculated using 2D forward modelling and 3D restorations, is also compared with fracture attribute data in order to determine any variations in fracture attributes in high and low strain regions.

3.2. Uncertainty

Errors in data collection are incurred for all fracture attributes, as well as grain size and simple curvature. Individual fracture lengths and spacing have been measured to the nearest 5 cm and apertures to the nearest 0.5 mm. Fracture lengths may be censored if the length of an individual fracture trace exceeds the extent of the outcrop; this usually affects only a small percentage of fractures because most fractures in this study are short compared to the size of the outcrop. Aperture measurements are likely to have additional errors due to erosion and fracture widening, however a value for this error is not known. A minimum number of 30 *n* points has been set to ensure fracture set orientation data is representative (see Watkins et al., 2015).

An average value for grain size is assigned to each sampling site; this is estimated from the exposure within the sampling circles, subject to exposure quality being good enough for a clean surface to be assessed. The average grain size at each sampling site is assigned to a category (150 μm, 187 μm, 219 μm, 250 μm, 313 μm, 375 μm, 435 μm, 500 μm, 625 μm, 750 μm, 875 μm, 1000 μm & 1500 μm) based on standard grain size card classes and intermediate classes for sand. Although the average grain size changes little in Torridon Group beds, sorting can be poor due to a fluvial depositional environment; this may cause significant errors in average grain size values, which have not been quantified.

Errors for simple curvature are also difficult to define; values are measured to three decimal places directly from Torridon Group surfaces in the 3D model. The major source of error arises from the 3D model building process. 3D surfaces are created by projection between adjacent cross sections; the model building algorithm used ensures the surface is a smooth fold shape, where bedding dip gradually changes. This process 'irons out' any kinks that would appear to be present due to bedding measurement errors or natural heterogeneity of the folded bedding surface; this means the 3D fold surfaces may not exactly match fold geometries on cross sections or in the field. In theory this should reduce error in simple curvature measurements but will smooth out natural perturbations and kinks that may influence strain and fracturing. Errors in simple curvature measurements due to incorrect 3D model fold geometries are most likely to occur in regions where outcrop is sparse, and therefore bedding data used to build 3D models is limited.

Watkins et al. (2015) test the intensity estimator of Mauldon et al., 2001 against actual fracture intensity values measured in the field. The study finds a very good correlation between the two datasets ($R^2 = 0.9837$). This means that the Mauldon method (Mauldon et al., 2001) can be used to identify overall trends in fracture intensity and determine how intensity varies depending on structural position (Watkins et al., 2015).

4. Strain modelling

Strain distribution during fold-thrust belt evolution varies depending on the active thrusting mechanism. End member models for thrust mechanisms include detachment folding (Poblet and McClay, 1996), fault propagation folding (Suppe and Medwedeff, 1990), trishear (Erslev, 1991), fault bend folding (Suppe, 1983) and fault parallel flow (Egan et al., 1997; Kane et al., 1997). Each mechanism creates folds of different geometries, and strain distributions are dependent on the folding mechanism; this has been shown in model folds (Salvini and Storti, 2001). Fracture distribution is affected by strain distribution, as well as mechanical layer properties (Cosgrove and Ameen, 2000); homogeneous isotropic layers undergo tangential longitudinal strain folding causing outer arc extension and inner arc compression in hinges, and limited deformation in limbs (Ramsay, 1967; Cosgrove and Ameen, 2000). Homogeneous anisotropic layers may undergo flexural slip or flexural flow where bedding-parallel slip leads to shearing in fold limbs and relatively undeformed hinges (Ramsay, 1967; Cosgrove and Ameen, 2000).

Using cross section forward modelling we illustrate the difference in three of the above thrusting mechanisms; fault parallel flow, fault bend folding and trishear. Fault bend folds are formed by displacement on a simple ramp-flat geometry fault, where the shape of the fold is purely due to the shape of the underlying thrust (Suppe, 1983). Bed thickness and length are conserved during hangingwall deformation (Medwedeff and Suppe, 1997). Fault parallel flow is similar to fault bend folding, however deformation is accommodated by fault-parallel shear (Kane et al., 1997; Egan et al., 1997), meaning bed thickness is not necessarily preserved. Trishear is a type of fault propagation folding mechanism where the thrust tip propagates as the fold develops (Erslev, 1991). Strain is distributed in a triangular zone in front of the thrust tip (trishear zone); there is a gradual decrease in fault slip velocity between the hangingwall and footwall. This gives folds curved geometries, and in some cases causes bed overturning (Erslev, 1991).

Section B–B′ (Fig. 5a) shows the geometry of the southern Achnashellach Culmination (see Fig. 2a for section line); three different forward modelling algorithms are used to recreate these fold geometries from a restored section and strain circles are used to highlight differences in strain distribution. The fault parallel flow mechanism (Fig. 5b) shows highest strain associated with thrust steepening and outer arc extension in upper units. Fault bend fold forward modelling (Fig. 5c) shows much higher strains than the previous model (Fig. 5b); strain is highest where thrust geometries are complex. Combined trishear and fault parallel flow indicate strains are generally low in backlimbs, even where thrusts are complex, and the highest strains are found in front of thrust tips and in forelimb regions (Fig. 5d). The differences in strain distributions in Fig. 5 show that it is important to determine the most realistic mechanisms of thrusting and fold formation in order to understand how strain evolves and is distributed.

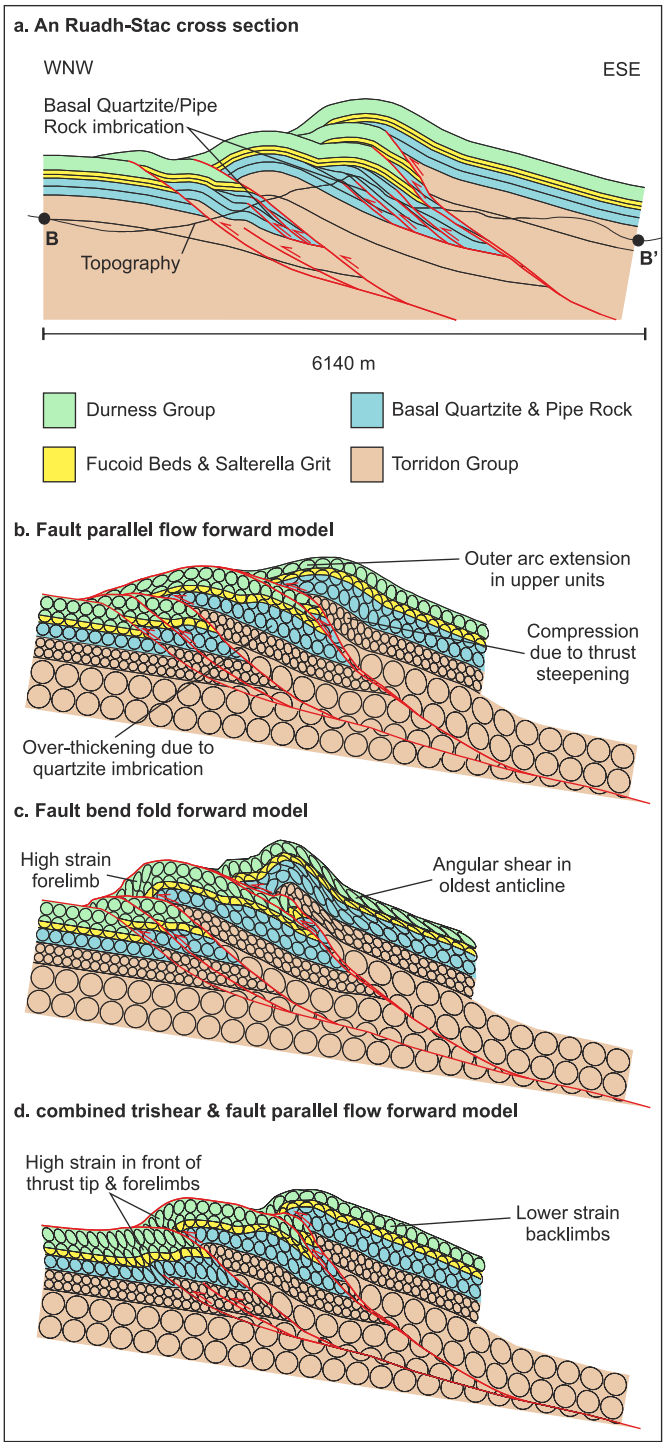

Fig. 5. a. An Ruadh-Stac cross section (B–B′, Fig. 2a). **b**. Forward modelling by fault parallel flow to recreate original section geometry (Fig. 5a). **c**. Forward modelling by fault bend folding. **d**. Forward modelling by combined trishear & fault parallel flow.

4.1. Cross section forward modelling

In order to determine the most appropriate end member thrust mechanism for the Achnashellach Culmination we compare the forward modelled top Torridon Group horizons (Fig. 5b–d) with those of the original section (Fig. 5a). We find the geometry of the combined trishear and fault parallel flow model (Fig. 5d) best represents the top Torridon Group horizon on the original section (Fig. 5a), so infer that this was the most likely thrust mechanism active during the evolution of the Achnashellach Culmination. This test was also undertaken on the Sgorr Ruadh section (A–A′, Fig. 2); the combined trishear and fault parallel flow forward modelling mechanism was found to best re-create fold geometries on the original Sgorr Ruadh cross section.

Forward modelling is applied to the Sgorr Ruadh section (A–A′, Fig. 2a) in order to determine strain distribution and identify how strain relates to fold simple curvature and structural position in the main fracture data collection region. Initially the cross section (Fig. 6a) is restored using line-length restoration (Dahlstrom, 1969);

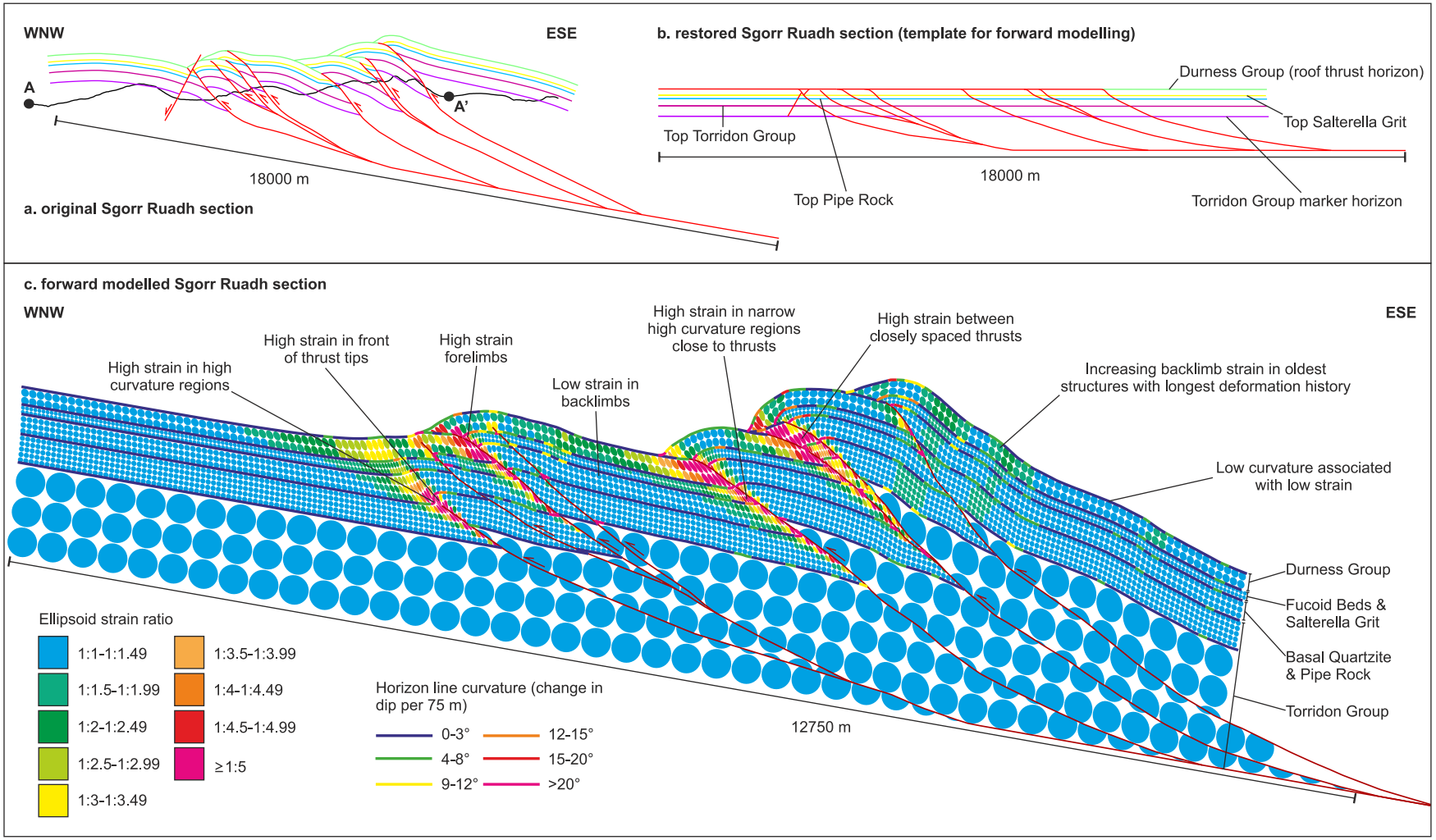

Fig. 6. **a**. Sgorr Ruadh cross section (A–A′, Fig. 2a). **b**. Restored-state Sgorr Ruadh cross section, used as a template for forward modelling. **c**. Forward modelled Sgorr Ruadh cross section to recreate original section geometries (Fig. 5a).

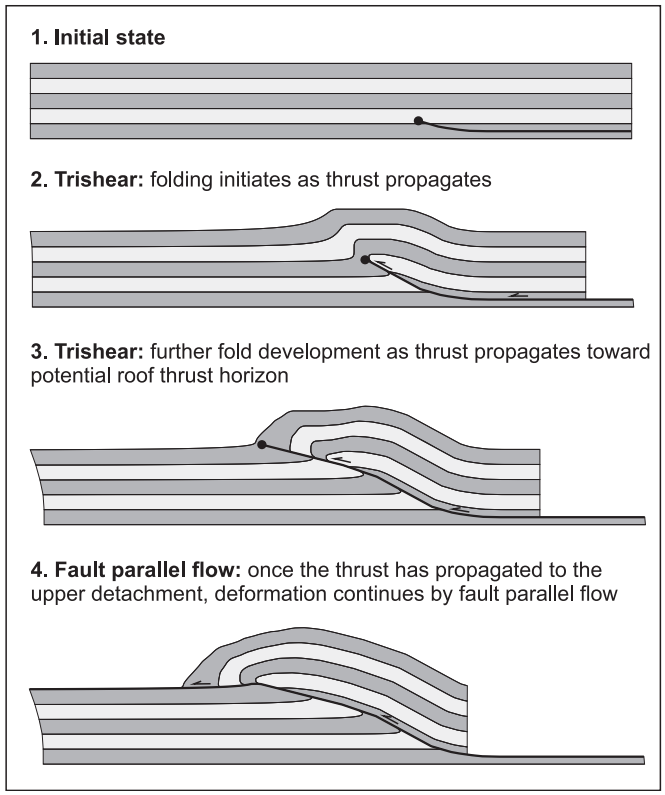

Fig. 7. Forward modelling workflow for combined trishear and fault parallel flow thrusting.

the restored state section (Fig. 6b) is then used as a template for forward modelling to ensure that the locations and geometries of thrusts are accurate. A foreland propagating thrust sequence is used for forward modelling; on each thrust the trishear thrusting mechanism is applied, and if the thrust tip propagates to the level of the roof thrust, further deformation is accommodated by fault parallel flow (Fig. 7).

The forward modelled Sgorr Ruadh section (Fig. 6c) illustrates the strain distribution predicted by the forward model through the fold and thrust belt. High strains are modelled in front of thrust tips, on fold forelimbs, and in narrow footwall and hanging wall zones close to thrusts. Strain is generally low in backlimb regions; however an overall increase in backlimb strain is seen to the ESE in structures that have undergone a longer deformation history. Age of fold structures is used as a proxy for strain and deformation history, where older structures (closer to the ESE hinterland) are inferred to have undergone higher strain. Fig. 6c also shows a clear relationship between strain and simple curvature; strain is generally highest in high curvature regions. Simple curvature is seen to increase in fold forelimbs, in front of thrust tips and in hangingwall and footwall positions, where strain is high. Lower simple curvature backlimbs are associated with lower strains.

4.2. 3D model restoration

Folds and faults in the study area change geometry along strike so in order to determine how strain is distributed in 3D we must consider 3D modelling of fold surfaces. This is completed, firstly by creating a series of closely spaced cross sections parallel to the regional transport direction, using bedding data to create the top Torridonian horizon lines and thrust lines. From these lines 3D surfaces are created (see Fig. 4 for 3D model and Fig. 2a for location of the 3D model); fault displacements are restored and anticlines are unfolded. Strain associated with the restoration is calculated and colour mapped onto the surfaces.

Fig. 8a shows the strain distribution for Anticline 4 (region x, Fig. 2a); the region of highest strain is found in the forelimb, associated with unfolding of a high simple curvature region (Fig. 8b). A rapid decrease in strain is seen through the fold hinge into the backlimb. Backlimb strain is very low, corresponding to low backlimb simple curvature (Fig. 8a and b). Linear strain trends seen on the backlimb are an artefact of the restoration process relating to the WNW transport direction used, and do not reflect actual strain patterns. 3D modelling reinforces the correlation between strain and simple curvature predicted using 2D forward modelling; this relationship is also seen in 3D on Anticlines 2–4 where increases in strain are found in regions of elevated simple curvature.

4.3. Predicting fracture attributes from simple curvature

From 2D forward modelling (Figure 6) and 3D restoration (Fig. 8) we have established that high strain is associated with high simple curvature. From this relationship we can begin to predict variations in fracture attributes depending on structural position. High strain, high simple curvature regions such as fold forelimbs and areas in close proximity to thrust planes are expected to contain high intensity, long fractures with wide apertures (e.g. Fig. 1). Lower strain, low simple curvature regions such as fold backlimbs are expected to contain lower intensity, shorter fractures with narrow apertures (e.g. Fig. 1). Since fracture orientation is thought to be related to stress orientations (Price, 1966) we would expect fracture orientations to be similar, regardless of structural position. The folds all formed during the same compressional event meaning regional stresses were relatively constant. However since high simple curvature regions have undergone significant outer arc stretching during folding we may expect well developed hinge-parallel fractures (J1 fractures, Fig. 1, Price, 1966).

5. Field fracture attributes

Sampling site localities discussed below are shown on Fig. 4 at their correct structural position. These sites are only a small sample of the total data set. These data have been chosen because they are a good representation of fracture distributions observed throughout the whole dataset, and exhibit fracture characteristic patterns observed throughout the fold belt.

Fractures observed in the Torridon Group sandstone are mostly joints, with a very limited number of shear fractures. As a result fracture offsets are rare. Fractures lack any systematic termination relationships between different fracture sets, meaning it is very difficult to determine relative ages. The Torridon Group foreland contains multiple fracture sets that appear not to be related to Moine Thrust Belt structures but instead formed either before or after folding and thrusting (Ellis et al., 2012). Measured intensities of these fractures are very low (<10 m/m^2). Since fractures in the Achnashellach Culmination lack cross-cutting or consistent termination relationships, it is not possible to determine which fractures are fold-related and which may be related to other events. However since the intensities of these non-fold related fractures are so low it is assumed that they will not have a significant impact on our results.

5.1. Orientation

Orientation data from each circular scan line is presented on equal area projections as contoured poles to fracture planes (Fig. 9).

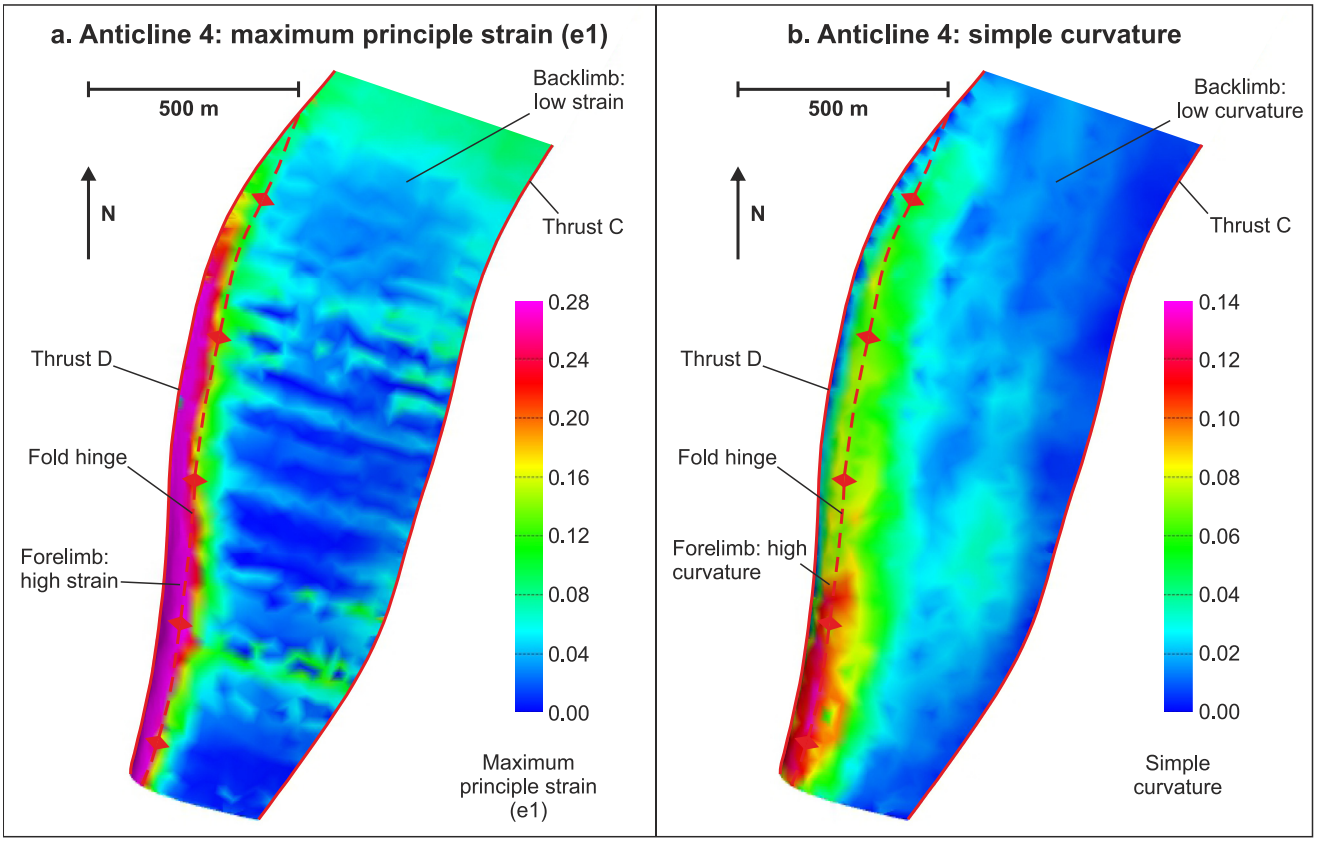

Fig. 8. **a**. Maximum principle strain (e1) for Anticline 4 (zone x, Fig. 2a), calculated by 3D model restoration in Move software. **b**. Simple curvature on a 3D surface for Anticline 4 (zone x, Fig. 2a), calculated using Move software.

Fractures have been unfolded relative to bedding for comparison purposes.

Regions of high simple curvature, such as the forelimb of Anticline 4, have a dominant fracture set striking parallel to the fold hinge (see sites A & B, Fig. 9). These are tension fractures equivalent to Price's J1 fracture set (Fig. 1, Price, 1966). Other fractures at different orientations can be seen in the high simple curvature regions but they are not as abundant. This J1 fracture set can be seen at all observed outcrops within the forelimb of Anticline 4 and has a consistent orientation throughout. The correlation of orientation data between adjacent sampling sites in high simple curvature regions is good (sites A & B, Fig. 9). Although the orientation of this fracture set is consistent along strike, the Fisher dispersion values are highly variable (46–114 for sites A & B, Fig. 9); this is because fractures are typically not straight.

In lower simple curvature regions we find fracture set orientations are very inconsistent, even over short distances (50 m between sites E & F, Fig. 9). It could be argued that the presence of non-fold related fractures could affect the orientation distributions, however as we have already stated, that intensity of these fractures in the foreland is so low that they should not significantly affect the overall orientation distribution in the fold and thrust belt. Some sampling sites contain fracture sets whose orientations relate to fold geometry (e.g. sites C & E have two sets parallel and perpendicular to fold hinges, J1 & J2 on Fig. 9, 63 & 134 Fisher dispersion), but often fractures are dispersed with no dominant clustering (e.g. sites D, F & G, Fig. 9, 87, 75 & 59 Fisher dispersion values). Dispersion of fracture orientations, along with a lack of evidence for relative timing of fracture formation, means it is not possible to divide fractures into individual sets.

Anticlines 2, & 4 comply with a relationship whereby high curvature simple regions have consistent fracture set orientations and lower curvature regions do not. Fracture orientation data on Anticline 1 is consistent across the entire structure; all sampling sites exhibit a J1 fracture set parallel to the fold hinge and a J2 fracture set parallel to the thrust transport direction (sites H, I & J, Fig. 9), despite having low simple curvature limbs (Fig. 4). Fisher dispersion values are consistently high throughout Anticline 1 (115 average Fisher dispersion for sites on Anticline 1), meaning that data scatter is minimal.

5.2. Length & aperture

Field data shows a relationship between fracture length and structural position. Individual sampling sites in high simple curvature regions consistently show fractures are mostly short (less than 0.5 m) (e.g. sites J & A, Fig. 10). Lower simple curvature regions commonly exhibit a mixture of long and short fractures and there appears to be no particular pattern for length distribution (e.g. sites K, L, M & N, Fig. 10). Fig. 11a shows a weak trend between fracture length and simple curvature, where high simple curvature regions have low average fracture lengths and the longest average fracture lengths are found in low simple curvature regions. Lengths also vary depending on the age of the fold on which the sampling site is located. The highest average fracture lengths (up to 2.75 m) are found on Anticlines 1 & 2, which are the oldest two structures, despite simple curvature in these regions being low. The youngest two structures (Anticlines 3 & 4) have

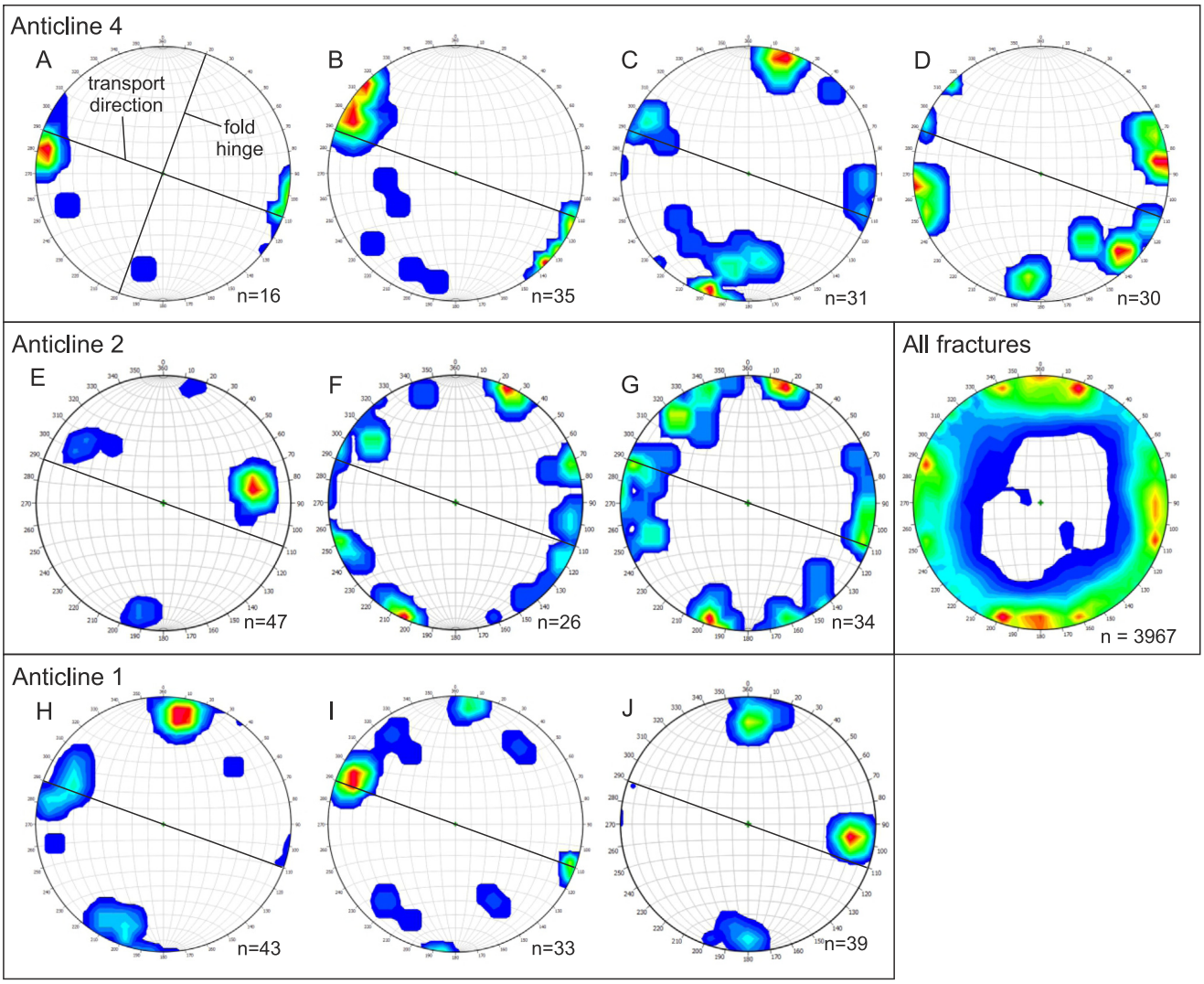

Fig. 9. Equal-area and lower-hemisphere projections showing contours of poles to fracture planes; fractures have been unfolded relative to bedding for comparison purposes. Sampling site locations are shown on Fig. 4. Sites in high simple curvature regions have consistent fracture orientations (A & B), whereas in low simple curvature regions fracture orientations are dispersed and inconsistent (C–G). Sampling sites on Anticline 1 are consistent across the entire structure (H–J). Data is colour mapped above 1% density, using a 1% contour interval for sites A–J. Data is colour mapped above 0.25% density, using a 0.25% contour interval for the 'All Fractures' plot. (For interpretation of the references to colour in this figure legend, the reader is referred to the web version of this article.)

much shorter average fracture lengths, with maximum values of only 1.2 m.

Average fracture length and average fracture aperture are compared on Fig. 11b. Although correlations between fracture length and aperture are observed in other field locations (e.g. Vermilye and Scholz, 1995; Ellis et al., 2012), no clear relationship is seen, and a poor coefficient of correlation is calculated ($R^2 = 0.0368$). This may be due to errors in aperture measurements; data is taken from glacially scoured bedding planes meaning that some fractures have been widened by erosion so aperture data is ambiguous. The average ratio of fracture aperture to length has been calculated as 0.0006 by plotting fracture length vs aperture for individual sampling sites (i.e. a fracture 1 m long will have an aperture of roughly 0.6 mm). This ratio varies depending on the grain size at each sampling site; coarser grained rocks have the narrowest fractures per unit length, and the widest apertures per unit length are found in fine grained rocks.

5.3. Intensity

Fracture intensity values, calculated using the Mauldon method (equation (1), Mauldon et al., 2001), and simple curvature show a very weak trend (Fig. 12). In general fracture intensity increases with increasing simple curvature but data is significantly scattered. A contour map for Anticline 4 (Fig. 13) shows a band of high fracture intensity in the high simple curvature forelimb (see Fig. 4), running parallel to the fold hinge. Fracture intensity gradually decreases into the backlimb, where intensity values are generally lower suggesting simple curvature is a key controlling factor on fracture intensity. Intensity values in the backlimb of Anticline 4 are highly variable; these variations do not relate to variations in simple curvature or strain as simple curvature is consistently low.

The intensity variability in low simple curvature zones may be caused by factors other than simple curvature variations such as lithology. A weak trend is seen between fracture intensity and grain size (Fig. 14a); intensity is consistently low in coarser grained rocks

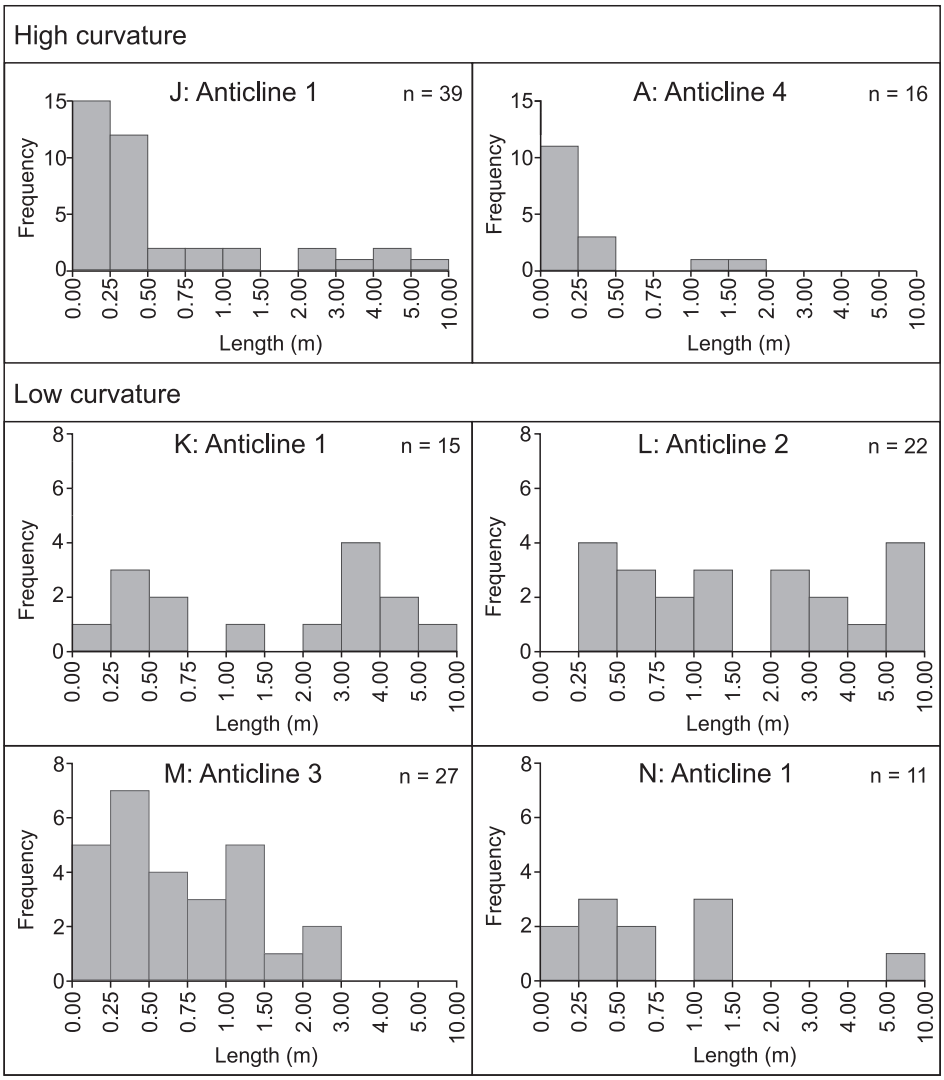

Fig. 10. Histograms for fracture length at individual sampling sites (localities shown on Fig. 4). Sites in high simple curvature regions contain very short fractures (J & A), whereas lower simple curvature regions have a mixture of long and short fractures and no clear length distribution pattern in seen (K–N).

and the highest fracture intensities are found in fine grained rocks. If data is divided according to the average grain size at each sampling site (Fig. 14b–d) the trend between simple curvature and fracture intensity strengthens (R^2 values are higher in Fig. 14 than in Fig. 12). This data suggests that fracture intensity may be controlled by both fold simple curvature and lithological variations.

5.4. Spatial distribution

The spatial distribution of fractures is affected by fracture orientation, length, intensity and fracture spacing. Fracture trace maps, created by digitising fractures on bedding planes from field photographs, show distinct differences between high and low simple curvature regions. Fig. 15a shows fracture patterns on two adjacent bedding planes in a high simple curvature region on Anticline 1 (location y, Fig. 2a). Fracture orientations, lengths, intensity and spacing are relatively consistent across both bedding planes and any change in the fracture distribution occurs gradually.

In low simple curvature regions fracture distributions can change significantly over short distances, shown by two adjacent bedding planes in a low simple curvature region of Anticline 2 (location z, Fig. 2a). Bedding plane 'b' (Fig. 15b) contains two main orthogonal fracture sets which are long and often form clusters of fractures. Fracture intensity on bedding plane 'b' is low. Bedding plane 'c' (Fig. 15c) contains three fracture sets, most of which are short with variable spacing. Intensity on bedding plane 'c' is much higher than on bedding plane 'b', despite the two being only 2 m apart.

6. Discussion

From previous work documenting structural controls on fracture attributes (e.g. Price, 1966; Hobbs, 1967; Jamison, 1997; Bergbauer and Pollard, 2004; Ortega et al., 2010; Barbier et al., 2012; Awdal et al., 2013) we predicted an increase in strain would lead to increased fracture intensity, length and aperture. Fracture orientations were predicted to be similar throughout the fold belt, with well-developed hinge-parallel fractures in high strain regions. Using 2D forward modelling and 3D restorations, high simple curvature regions were predicted to have undergone high strain during folding and thrusting. From this inferred relationship it was predicted that fracture intensity, length and aperture of hinge-parallel fractures would increase in high simple curvature regions such as fold forelimbs and close to thrust planes.

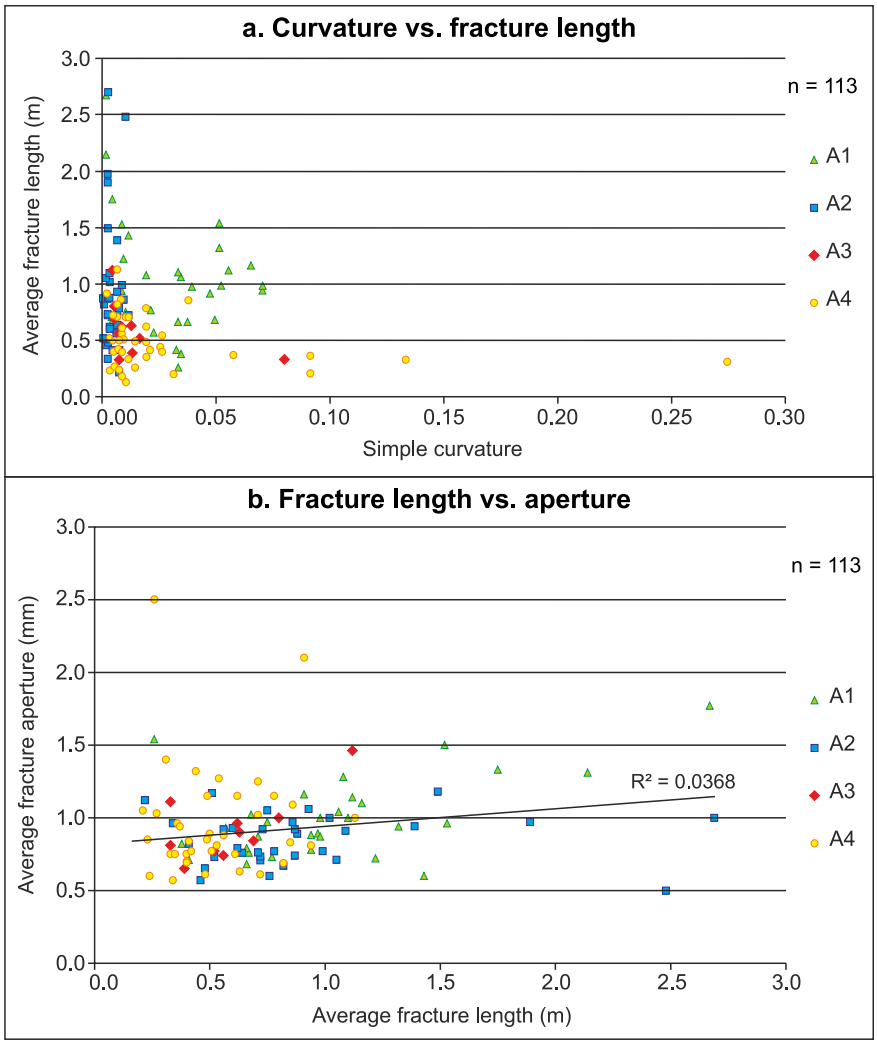

Fig. 11. **a**. Scatter graph of simple curvature versus fracture length; the highest simple curvature regions have the lowest average fracture lengths and the highest average fracture lengths are found in low simple curvature regions. Folds with longer deformation histories (used as a proxy for strain history) (Anticline 1 & 2 (A1 & A2)) have the longest average fracture lengths and younger folds (Anticline 3 & 4 (A3 & A4)) have much shorter average fracture lengths. **b**. Scatter graph of average fracture length versus average fracture aperture; no correlation is seen.

Field data confirms a relationship between fracture attribute variations and structural position within a fold-and-thrust belt. Within high simple curvature regions a single dominant fracture set is observed, striking parallel to the fold hinge; these are tension fractures that have formed as a direct result of the folding process. This fracture set is most abundant in high simple curvature regions as these have undergone the most outer arc stretching during folding, which has resulted in the fractures' formation. The presence of only a single dominant fracture set suggests high simple curvature regions were constantly in WNW-ESE tension throughout the folding process. This meant that only one of the four fracture sets that might be expected on a thrust-related anticline (Price, 1966) were able to form (Fig. 16).

Fractures in high simple curvature regions are mostly short (Fig. 16); the dominant, hinge-parallel fractures tend to be less than 0.5 m long. In order to accommodate stretching during folding fractures either may propagate in both length and aperture or additional short fractures may form. This paper hypothesised that high strain in high simple curvature regions may be accommodated by longer fractures. It is probable that, rather than fracture propagation, strain was accommodated through the formation of new fractures; fracture intensity is consistently high in regions of high simple curvature (Fig. 16). This is because higher fracture intensities were needed to accommodate the high strains associated with the folding process. Since fracture set orientations in high simple curvature regions are consistent, we infer stress during fracturing was high and localised, creating fracture characteristics that show little variation along strike.

In low simple curvature regions fracture set orientations are highly variable and inconsistent along strike (Fig. 16). Even within a single data sampling circle fracture sets often show significant orientation dispersion. In these regions multiple fracture sets are seen at each outcrop, although no dominant set can be identified across larger areas. Fracture lengths in low simple curvature regions are generally longer than in high simple curvature areas (Fig. 16). Low simple curvature regions tend to exhibit lower fracture intensities than high simple curvature areas, however we see significant variations over short distances (Fig. 16) indicating simple curvature may not be the only controlling factor. Previous researchers have suggested lithology may influence fracture intensity (e.g. Hugman and Friedman, 1979; Corbett et al., 1987; Hanks et al., 1997; Wennberg et al., 2006; Ferrill and Morris, 2008; Ortega et al.,

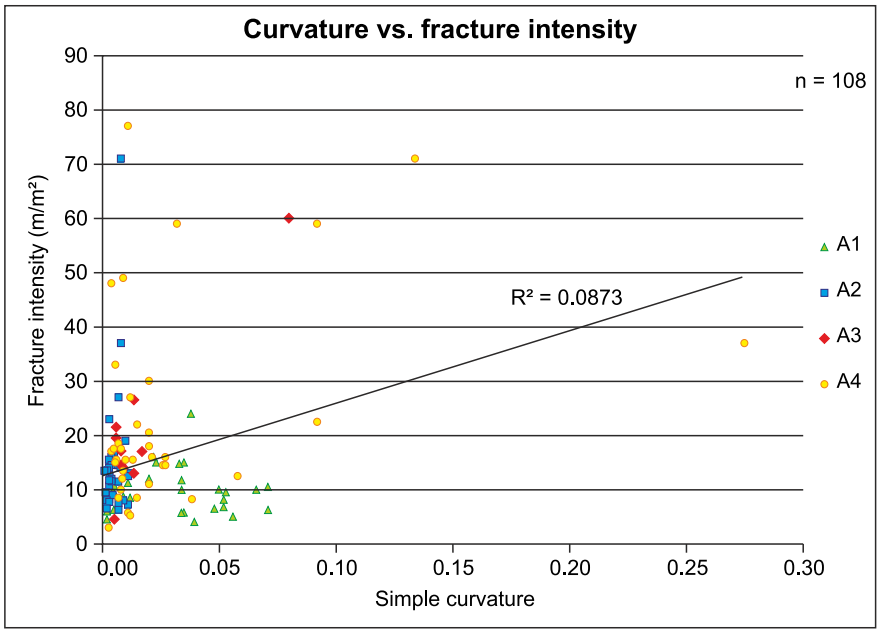

Fig. 12. Scatter graph of simple curvature versus fracture intensity; a weak trend is shown.

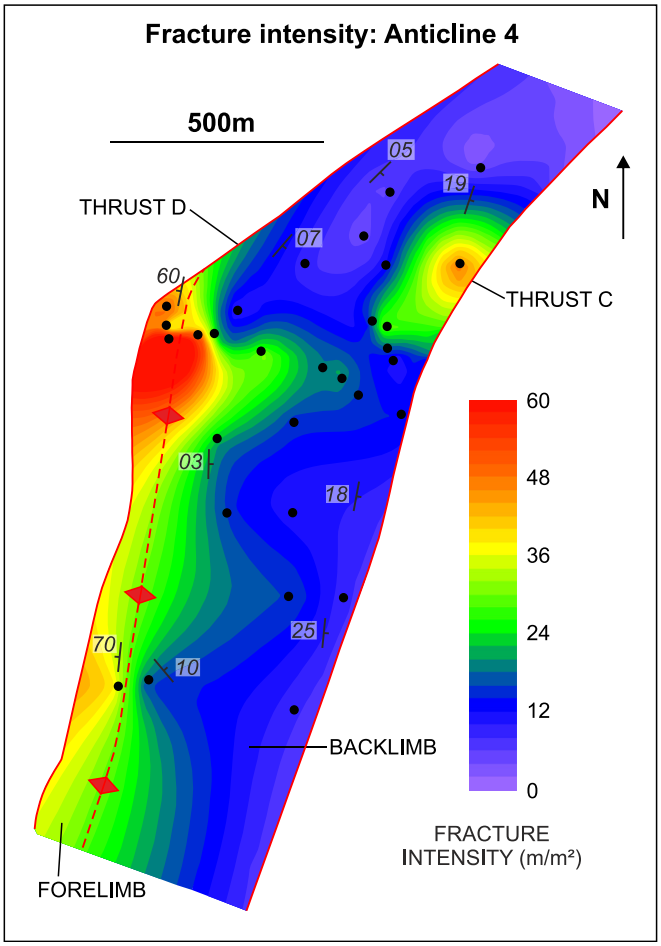

Fig. 13. Contour map of Anticline 4 (region x, Fig. 2a) showing the high fracture intensity in the forelimb and lower fracture intensity in the backlimb.

2010; Barbier et al., 2012); we see evidence for this in low simple curvature regions as lower fracture intensities are found at sampling sites with coarse grain sizes. This variability in fracture intensity may be caused by pre-failure strain variations where microstructural deformation accommodates strain before brittle failure and fracturing occurs. Mechanisms of pre-failure strain may include micro-fracturing, pressure solution, cataclastic flow as well as the formation of undulose extinction, deformation lamellae and deformation twinning and kinking (Passchier and Trouw, 2005). Certain lithological characteristics may allow for higher strains to be accommodated by these mechanisms prior to brittle fracturing, which could mean lower fracture intensities are seen at outcrop. The scatter of fracture orientation data in low curvature regions suggests strain was dispersed during folding, and the variability in fracture intensity suggests strain was low enough for lithological factors to influence fracture formation.

Field evidence shows that fold simple curvature has an influence on fracture characteristics; fractures in high simple curvature regions are primarily controlled by strain and are relatively predictable. Fractures in low simple curvature regions are highly variable and may be controlled by a combination of strain and lithological variations, such as grain size. However, the relationships between fracture length and intensity with simple curvature, and fracture intensity with grain size (Figs. 11a, 12 and 14) are weakly constrained, indicating other factors are partially controlling fracture attributes. For example distance to major faults or lithological factors other than grain size are seen to affect fracture intensity in other regions. These observations have been made at other field locations, where the influence of structural controls on fracturing increases as strain increases. Barbier et al. (2012) suggest structural position is important for fracture intensity on the Sheep Mountain Anticline, Wyoming; the forelimb and crest have higher fracture intensities than the backlimb. The authors suggest fracture intensities on the relatively undeformed backlimb are stratigraphically, rather than structurally controlled. Hanks et al. (1997) suggest that fracture intensity variations in the Lisburne Group, Northeast Alaska, are controlled by changes in rock composition, grain size & texture, however structural position influences fracturing in deformed regions. We suggest that in deformed regions

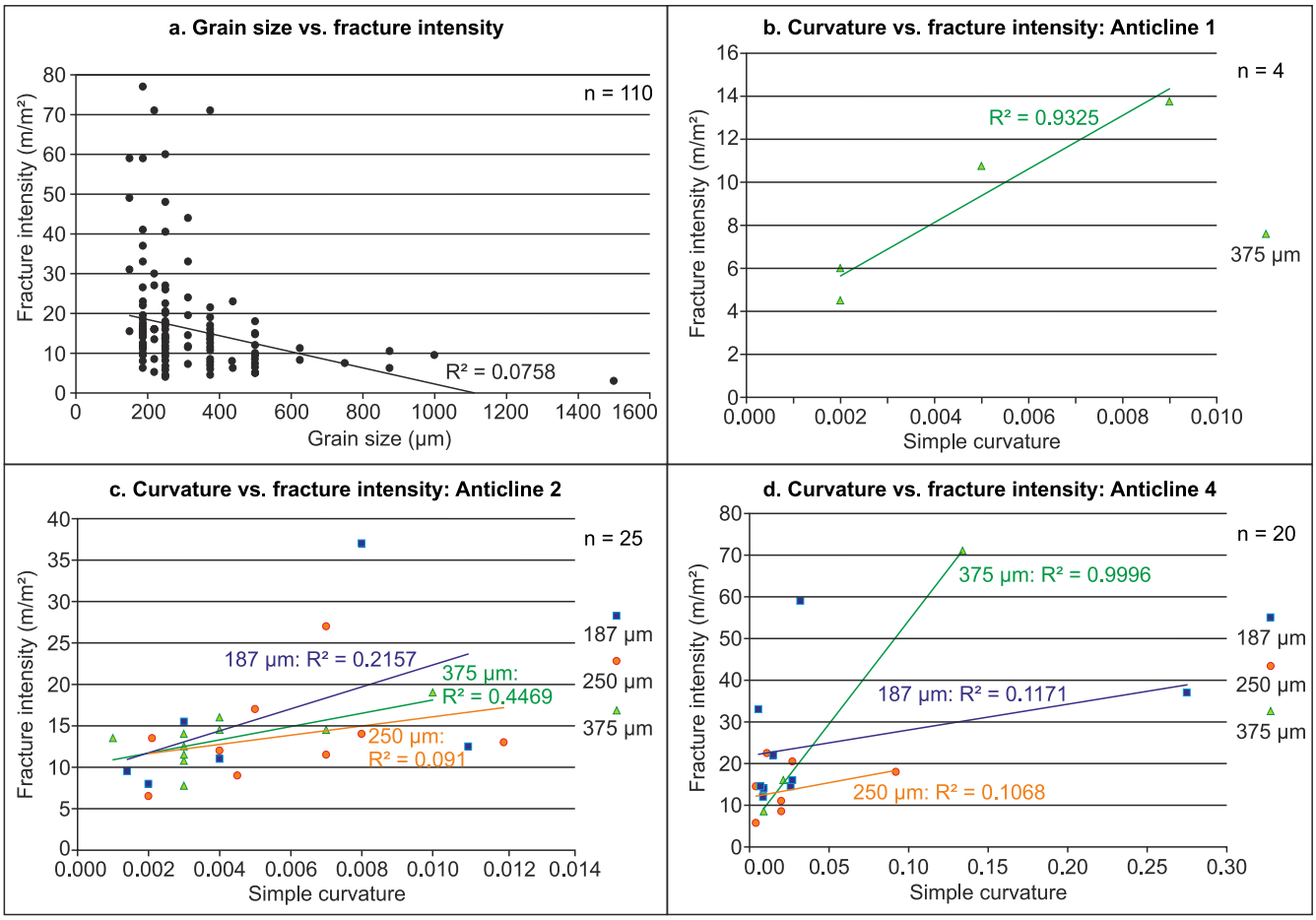

Fig. 14. **a**. Scatter graph of grain size versus fracture intensity; higher grain sized rocks consistently show very low fracture intensities and the highest fracture intensities are found in very fine grained rocks. **b**–**d**). Scatter graphs of simple curvature versus fracture intensity; dividing data by grain size shows that the trend between simple curvature and fracture strengthens slightly (compared with Fig. 12).

such as folds, lithology may still influence fracture intensity but structural position becomes increasingly important as strain increases.

As well as fold simple curvature playing an important role in controlling fracture characteristics, we have seen that the deformation history of fold structures may also be important. Although Anticline 1 has very straight, low simple curvature limbs we see that fracture orientations are consistent across the entire fold. Anticline 1 is inferred to be the oldest fold within the sampling region, and therefore has the longest deformation history. It is possible that, following initial folding due to displacement on Thrust A (see Fig. 2a), Anticline 1 was then passively folded due to uplift associated with the formation of Anticlines 2–4. This means the present day simple curvature observed on Anticline 1, especially in the forelimb, may be slightly lower than it was prior to the formation of Anticlines 2–4, and, in this case, is not a good predictor of strain history.

Length of deformation history appears to have influenced other fracture characteristics, namely fracture length. The highest fracture lengths are found in the two oldest anticlines (Anticline 1 & 2) and the shortest fractures are found in the youngest two anticlines (Anticline 3 & 4). Longer deformation histories of Anticlines 1 & 2 mean they have undergone more passive bending due to the formation of underlying, younger folds. This is because, in a foreland propagating sequence, Anticline 1 has undergone passive deformation by the formation of 3 underlying folds (Anticlines 2–4), which formed later than itself. Anticline 4, on the other hand, has undergone no passive deformation as it is the youngest structure and no folding has occurred in its footwall subsequent to its formation. Strain associated with this passive deformation may have been accommodated by length propagation and fracture widening of pre-existing fractures, rather than the formation of new fractures as fracture intensities are generally relatively low (Fig. 12).

7. Conclusions

Using cross section forward modelling, 3D model restorations and field fracture data we have inferred a combination of structural and lithological controls on fracture characteristic variations within the Achnashellach fold-and-thrust belt. Both fold simple curvature and deformation history have influenced fracture formation; ultimately both relate to strain, which is the key structural control on fracture attribute variation. Lithology may also play a role in influencing fracture development, and the importance of lithology varies depending on structural position. In low strain regions variations in fracture attributes are influenced by lithology changes; as strain increases lithology continues to influence fracture shape and intensity but structural position takes over as the most important controlling factor on fracture formation.

By using data collected from four anticlines, all of which have different geometries and deformation histories, we have highlighted the importance of sampling on multiple fold structures.

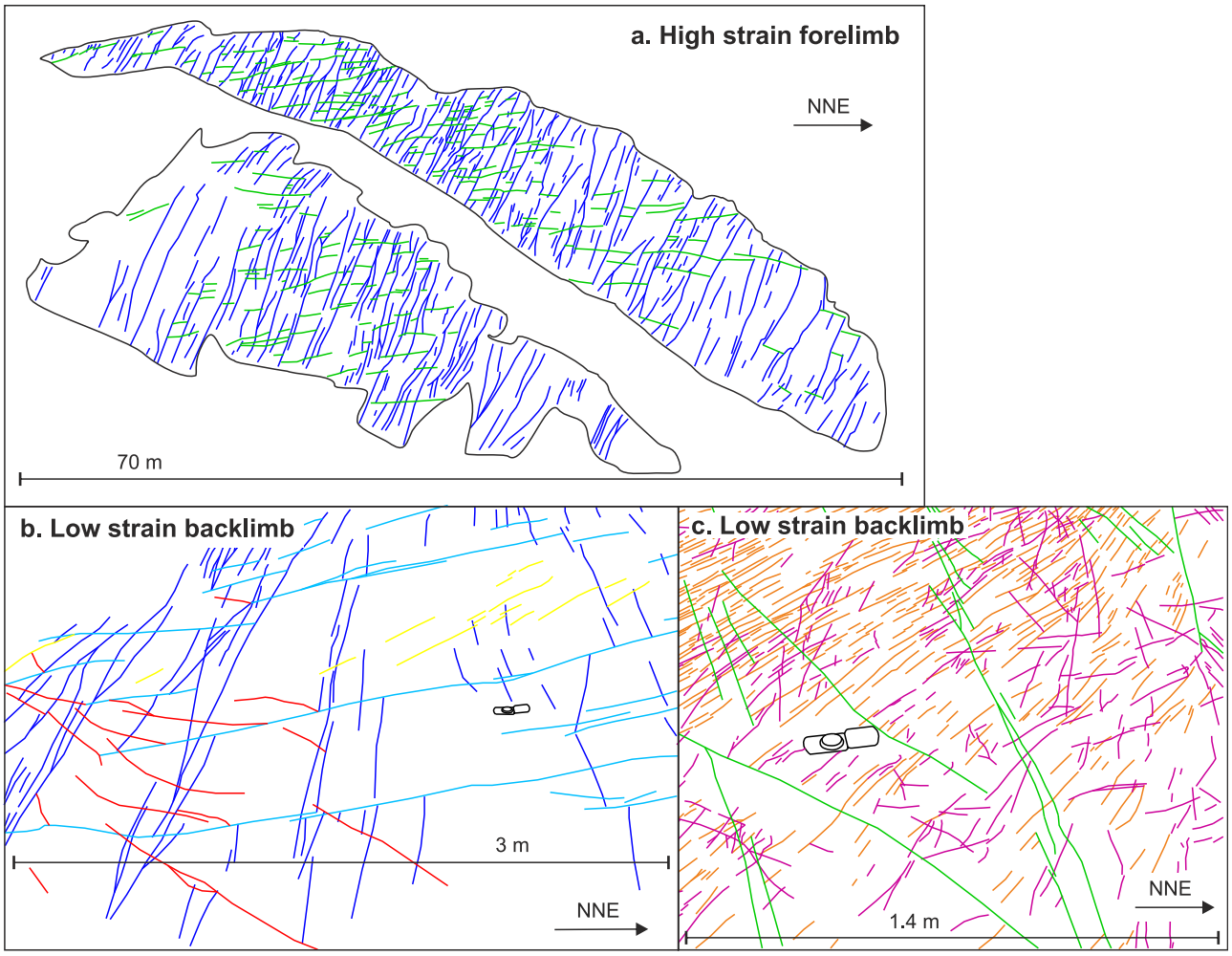

Fig. 15. **a**. Two bedding planes in a high strain region (y on Fig. 2a) have consistent fracture orientations, lengths, intensities and distribution. **b**. Two adjacent bedding planes in a low strain region (z on Fig. 2a), spaced 2 m apart. Fracture orientations are completely different despite being at the same structural position. Fracture trace maps are shown relative to the orientation of the fold hinge (NNE).

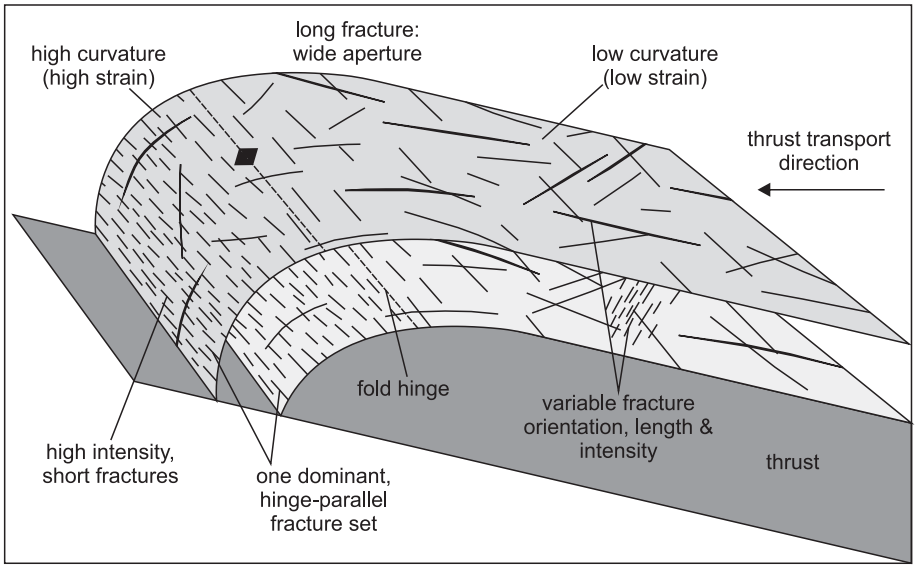

Fig. 16. Field data suggests high strain regions of thrust-related anticlines contain high intensity, short fractures which have relatively consistent orientations across large areas. In contrast to this low strain regions contain fractures with highly variable fracture intensities, lengths and orientations.

Sampling only Anticline 1 would indicate that deformation history is the key control as fractures are well developed across the entire structure, even though simple curvatures are generally low. Sampling only Anticlines 2 & 3 may suggest that lithological variations are the key control on fracture variations and structural controls play only a minor role. Sampling on only Anticline 4 would suggest fold simple curvature is the main influence on fracture pattern variations. This raises the question as to the efficiency of potential predictions of fracture attributes in adjacent structures or the subsurface from studies of single structures in a fold and thrust belt.

Acknowledgements

This research is funded by a NERC CASE studentship (NERC code NE/I018166/1) in partnership with Midland Valley. The authors thank Midland Valley for use of FieldMove Clino software for fracture data collection, and Move software for cross section construction, and strain modelling. 3D Field software is acknowledged for contour map creation. We also thank Toru Takeshita for overseeing the editorial process, and Catherine Hanks and Ole Petter Wennberg for constructive reviews.

References

Ameen, M.S., 2014. Fracture and in-situ stress patterns an impact on performance in the Khuff structural prospects, eastern offshore Saudi Arabia. Mar. Pet. Geol. 50, 166–184.
Awdal, A.H., Braathen, A., Wennberg, O.P., Sherwani, G.H., 2013. The characteristics of fracture networks in the Shiranish formation of the Bina Bawi Anticline; comparison with the Taq Taq field, zagros, Kurdistan, NE Iraq. Pet. Geosci. 19, 139–155.
Barbier, M., Hamon, Y., Callot, J., Floquet, M., Daniel, J., 2012. Sedimentary and diagenetic controls on the multiscale fracturing pattern of a carbonate reservoir: The Madison Formation (Sheep Mountain, Wyoming, USA). Mar. Pet. Geol. 29, 50–67.
Bellahsen, N., Fiore, P., Pollard, D.D., 2006. The role of fractures in the structural interpretation of Sheep Mountain Anticline, Wyoming. J. Struct. Geol. 28, 850–867.
Bergbauer, S., Pollard, D.D., 2004. A new conceptual fold-fracture model including prefolding joints, based on the Emigrant Gap anticline, Wyoming. GSA Bull. 116 (3/4), 294–307.
Butler, R.W.H., Matthews, S.J., Morgan, R.K., 2007. Structural evolution of the Achnashellach Culmination, southern Moine Thrust Belt: testing the duplex model. In: Ries, A.C., Butler, R.W.H., Graham, R.H. (Eds.), Deformation of the Continental Crust: the Legacy of Mike Coward, pp. 103–120. Geological Society, London, Special Publications, 272.
Cooper, M., 1992. The analysis of fracture systems in subsurface thrust structures from the Foothills of the Canadian Rockies. In: McClay, K.R. (Ed.), Thrust Tectonics. Chapman and Hall, London, pp. 391–405.
Corbett, K., Friedman, M., Spang, J., 1987. Fracture development and mechanical stratigraphy of Austin Chalk, Texas. AAPG Bull. 71 (1), 17–28.
Cosgrove, J.W., Ameen, M.S., 2000. A comparison of the geometry, spatial organization and fracture patterns associated with forced fold and buckle folds. In: Cosgrove, J.W., Ameen, M.S. (Eds.), Forced Fold and Fractures, pp. 7–21. Geological Society, London, Special Publications, 169.
Dahlstrom, C.D.A., 1969. Balanced cross sections. Can. J. Earth Sci. 6, 743–757.
Di Naccio, D., Boncio, P., Cirilli, S., Casaglia, F., Morettini, E., Lavecchia, G., Brozzetti, F., 2005. Role of mechanical stratigraphy on fracture development in carbonate reservoirs: insights from outcropping shallow water carbonates in the Umbria-Marche Apennines, Italy. J. Volcanol. Geotherm. Res. 148, 98–115.
Egan, S.S., Buddin, T.S., Kane, S.J., Williams, G.D., 1997. Three-dimensional modelling and visualisation in structural geology: new techniques for the restoration and balancing of volumes. In: Proceedings of the 1996 Geoscience Information Group Conference on Geological Visualisation. Electronic Geology, pp. 67–82. V. 1, Paper 7.
Ellis, M.A., Laubach, S.E., Eichhubl, P., Olson, J.E., Hargrove, P., 2012. Fracture development and diagenesis of Torridon Group Applecross Formation, near An Teallach, NW Scotland: millennia of brittle deformation resilience? J. Geological Soc. Lond. vol. 169, 297–310.
Erslev, E.A., 1991. Trishear fault-propagation folding. Geology 19, 617–620.
Ferrill, D.A., Morris, A.P., 2008. Fault zone deformation controlled by carbonate mechanical stratigraphy Balcones fault system, Texas. AAPG Bull. 92 (3), 359–380.
Florez-Niño, J.-M., Aydin, A., Mavko, G., Antonellini, M., Ayaviri, A., 2005. Fault and fracture systems in a fold and thrust belt: an example from Bolivia. AAPG Bull. 89 (4), 471–493.
Ghosh, K., Mitra, S., 2009. Structural controls of fracture orientations, intensity, and connectivity, Teton anticline, Sawtooth Range, Montana. AAPG Bull. 93 (8), 995–1014.
Guiton, M.L.E., Sassi, W., Leroy, Y.M., Gauthier, B.D.M., 2003. Mechanical constraints on the chronology of fracture activation in folded Devonian sandstone of the Western Moroccan Anti-Atlas. J. Struct. Geology 25, 1317–1330.
Hanks, C.L., Lorenz, J., Teufel, L., Krumhardt, A.P., 1997. Lithologic and structural controls on natural fracture distribution and behavior within Lisburne Group, Northeastern Brooks Range and North Slope Subsurface, Alaska. AAPG Bull. 81 (10), 1700–1720.
Hennings, P.H., Olson, J.E., Thompson, L.B., 2000. Combining outcrop data and three-dimensional structural models to characterize fractured reservoirs: an example from Wyoming. AAPG Bull. 84 (6), 830–849.
Hobbs, D.W., 1967. The formation of tension joints in sedimentary rocks: an explanation. Geol. Mag. 104 (6), 550–556.
Hugman, R.H.H., Friedman, M., 1979. Effects of texture and composition on mechanical behavior of experimentally deformed carbonate rocks. AAPG Bull. 63 (9), 1478–1489.
Iñigo, J.F., Laubach, S.E., Hooker, J.N., 2012. Fracture abundance and patterns in the Subandean fold and thrust belt, Devonian Huamampampa Formation petroleum reservoirs and outcrops, Argentina and Bolivia. Mar. Pet. Geol. 35, 201–218.
Jamison, W.R., 1997. Quantitative evaluation of fractures on Monkshood anticline, a detachment fold in the Foothills of Western Canada. AAPG Bull. 81 (7), 1110–1132.
Kane, S.J., Williams, G.D., Buddin, T.S., Egan, S.S., Hodgetts, D., 1997. Flexural-slip Based Restoration in 3D, a New Approach, 1997 AAPG Annual Convention Official Program, A58.
Lisle, R., 1994. Detection of zones of abnormal strains in structures using Gaussian Curvature Analysis. AAPG Bull. 78 (12), 1811–1819.
Lisle, R., 2000. Predicting patterns of strain from three-dimensional fold geometries: neutral surface folds and forced folds. In: Cosgrove, J.W., Ameen, M.S. (Eds.), Forced Folds and Fractures, pp. 213–221. Geological Society, London, Special Publications, 169.
Mauldon, M., Dunne, W.M., Rohrbaugh, M.B., 2001. Circular scanlines and circular windows: new tools for characterizing the geometry of fracture traces. J. Struct. Geology 23, 247–258.
McQuillan, H., 1973. Small-scale fracture density in Asmari Formation of Southwest Iran and its relation to bed thickness and structural setting. AAPG Bull. 57 (12), 2367–2385.
McQuillan, H., 1974. Fracture Patterns on Kuh-e Asmari Anticline, Southwest Iran. AAPG Bull. 58 (2), 236–246.
Mendum, J.R., Barber, A.J., Butler, R.W.H., Flinn, D., Goodenough, K.M., Krabbendam, M., Park, R.G., Stewart, A.D., 2009. Lewisian, Torridonian and Moine Rocks of Scotland, Geological Conservation Review Series, vol. 34. Joint Nature Conservation Committee, Peterborough.
Medwedeff, D.A., Suppe, J., 1997. Multibend fault-bend folding. J. Struct. Geology 19 (3–4), 279–292.
Mitra, S., 1988. Effects of deformation mechanisms on reservoir potential in Central Appalachian Overthrust Belt. AAPG Bull. 75 (5), 536–554.
Muecke, G.K., Charlesworth, H.A.K., 1966. Jointing in folded Cardium Sandstone along the Bow River, Alberta. Can. J. Earth Sci. 3, 579–596.
Nelson, R.A., 1985. Geologic Analysis of Naturally Fractured Reservoirs. Gulf Publishing, Houston, Texas.
Odling, N.E., Gillespie, P., Bourgine, B., Castaing, C., Chilés, J.-P., Christensen, N.P., Fillion, E., Genter, A., Olsen, C., Thrane, L., Trice, R., Aarseth, E., Walsh, J.J., Watterson, J., 1999. Variations in fracture system geometry and their implications for fluid flow in fractured hydrocarbon reservoirs. Pet. Geosci. 5, 373–384.
Ortega, O.J., Gale, J.F.W., Marrett, R., 2010. Quantifying diagenetic and stratigraphic controls on fracture intensity in platform carbonates: an example from the Sierra Madre Oriental, northeast Mexico. J. Struct. Geology 32, 1943–1959.
Pahl, P.J., 1981. Estimating the mean length of discontinuity traces. Int. J. Rock Mech. Min. Sci. Geomech. Abstr. 18, 221–228.
Passchier, C.W., Trouw, R.A.J., 2005. Microtectonics. Springer-Verlag Berlin Heidelberg.
Poblet, J., McClay, K., 1996. Geometry and kinematics of single layer detachment folds. Bull. Assoc. Pet. Geol. 80, 1085–1109.
Price, N.J., 1966. Fault and Joint Development in Brittle and Semi-brittle Rocks (Pergamon, Oxford).
Priest, S.D., 1993. Discontinuity Analysis for Rock Engineering. Chapman & Hall, London, United Kingdom.
Priest, S.D., Hudson, J.A., 1981. Estimation of discontinuity spacing and trace length using scanline surveys. Int. J. Rock Mech. Min. Sci. Geomech. Abstr. 18, 183–197.
Ramsay, J.G., 1967. Folding and Fracturing of Rocks. McGraw-Hill Book Company.
Salvini, F., Storti, F., 2001. The distribution of deformation in parallel fault-related folds with migrating axial surfaces: comparison between fault-propagation and fault-bend folding. J. Struct. Geology 23, 25–32.
Stewart, A.D., 2002. The Later Proterozoic Torridonian Rocks of Scotland: Their Sedimentology, Geochemistry and Origin. Geological Society, London, Memoirs, 24.
Storti, F., Salvini, F., 2001. The evolution of a model trap in the central Apennines, Italy: development of cataclastic rocks in carbonates at the Narni anticline. J. Pet. Geol. 24 (2), 171–190.
Suppe, J., 1983. Geometry and kinematics of fault-bend folding. Am. J. Sci. 283, 684–721.

Suppe, J., Medwedeff, D.A., 1990. Geometry and kinematics of fault-propagation folding. Eclogae Geol. Helvatiae 83, 409–454.
Vermilye, J.M., Scholz, C.H., 1995. Relation between vein length and aperture. J. Struct. Geology 17 (3), 423–434.
Watkins, H., Bond, C.E., Butler, R.W.H., 2014. Identifying multiple detachment horizons and an evolving thrust history through cross-section restoration and appraisal in the Moine Thrust Belt, NW Scotland. J. Struct. Geol. 66, 1–10.
Watkins, H., Bond, C.E., Healy, D., Butler, R.W.H., 2015. Appraisal of fracture sampling methods and a new workflow to characterise heterogeneous fracture networks at outcrop. J. Struct. Geol. 72, 67–82.
Wennberg, O.P., Svånå, T., Azizzadeh, M., Aqrawi, A.M.M., Brockbank, P., Lyslo, K.B., Ogilvie, S., 2006. Fracture intensity vs. mechanical stratigraphy in platform top carbonates: the Aquitanian of the Asmari Formation, Khaviz Anticline, Zagros, SW Iran. Pet. Geosci. 12, 235–245.
Wennberg, O.P., Azizzadeh, M., Aqrawi, M.M., Blanc, E., Brockbank, P., Lyslo, K.B., Pickard, N., Salem, L.D., Svånå, T., 2007. The Khaviz Anticline: an outcrop analogue to giant fractured Asmari Formation reservoirs in SW Iran. In: Lonergan, L., Jolly, R.J.H., Rawnsley, K., Sanderson, D.J. (Eds.), Fractured Reservoirs, pp. 23–42. Geological Society, London, Special Publications, 270.